Highly Simplified and Bandwidth-Efficient Human Body Communications Based on IEEE 802.15.6 WBAN Standard

Tae-Wook Kang, Jung-Hwan Hwang, Sung-Eun Kim, Kwang-Il Oh, Hyung-Il Park, In-Gi Lim, and Sung-Weon Kang

This paper presents a transmission method for improving human body communications in terms of spectral efficiency, and the performances of bit-error-rate (BER) and frame synchronization, with a highly simplified structure. Compared to the conventional frequency selective digital transmission supporting IEEE standard 802.15.6 for wireless body area networks, the proposed scheme improves the spectral efficiency from 0.25 bps/Hz to 1 bps/Hz based on the 3-dB bandwidth of the transmit spectral mask, and the signal-to-noise-ratio (SNR) by 0.51 dB at a BER of 10^{-6} with an 87.5% reduction in the detection complexity of the length of the Hamming distance computation. The proposed preamble structure using its customized detection algorithm achieves perfect frame synchronization at the SNR of a BER of 10^{-6} by applying the proposed pre-processing to compensate for the distortions on the preamble signals due to the band-limit effects by transmit and receive filters.

Keywords: Wireless body area networks, Human body communications, Frequency selective digital transmission.

I. Introduction

Human body communications (HBC) is an innovative wireless communication method that can be used to connect devices using the human body as a transmission medium [1], [2]. Using HBC, a simple touch or connection through the body can transfer data and create a wireless network among on-body, touch-and-play based devices, and in-body [3]–[6]. HBC can be considered as a suitable user interface to form links between wearable systems based on wireless body area networks (WBANs) and wide-range communications such as 5G networks.

The frequency selective digital transmission (FSDT) standardized in IEEE standard 802.15.6 for WBAN has been adopted in an HBC transmitter (Tx) [5]. The FSDT transmitted signal can be spread throughout a selected frequency domain centered on 21 MHz using a 42 MHz operating clock frequency f_{op} without a digital-to-analog converter, an analog-to-digital converter, or a radio frequency block. Hence, it can provide advantages in reducing the size for implementation, and low power consumption. The conventional FSDT from the standard specifications transmits data at a maximum data rate of 1.3125 Mbps. However, its maximum spectral efficiency is limited to 0.25 bps/Hz according to the 3 dB bandwidth $f_{3dB\text{-}BW}$ of the transmit spectral mask (TSM) requirement to cover the data chip rate of 5.25 Mcps [5]. Moreover, the bit-error-rate (BER) performance is degraded by the effects of the transmit filter due to inter-symbol interference (ISI) induced by the repeated binary patterns (RBPs) of '00' and '11' in the

Manuscript received Mar. 4, 2016; revised June 20, 2016; accepted July 25, 2016.

This work was supported by 'The Cross-Ministry Giga KOREA Project' grant from the Ministry of Science, ICT and Future Planning, Rep. of Korea.

Tae-Wook Kang (corresponding author, twkang@etri.re.kr), Sung-Eun Kim (sekim@etri.re.kr), Kwang-Il Oh (kioh@etri.re.kr), Hyung-Il Park (hipark@etri.re.kr), In-Gi Lim (iglim@etri.re.kr), and Sung-Weon Kang (kangsw@etri.re.kr) are with the ICT Materials & Components Research Laboratory, ETRI, Daejeon, Rep. of Korea.

Jung-Hwan Hwang (jhhwang@etri.re.kr) is with the Broadcastings & Medias Research Laboratory, ETRI, Daejeon, Rep. of Korea.

http://dx.doi.org/10.4218/etrij.16.2716.0003

transmitted signals [7]. Previous approaches based on FSDT have presented a parallelized multi-spreader [7], [8], multi-level baseband coding [9], and direct spreading using Walsh codes [10], but only considering an increase in throughput.

This paper proposes a narrow band digital transmission (NBDT), which can achieve a maximum spectral efficiency of up to 1 bps/Hz with robustness against the band-limit effects on the transmit signals by the transmit filter. Compared to the current FSDT, the NBDT improves the signal-to-noise-ratio (SNR) by about 0.51 dB at a BER of 10^{-6} with reduced detection complexity of the computation length of the Hamming distance (HD) per one information bit, and simplifies the Tx implementation by excluding a serial-to-parallel (S2P) block and memory required to store the orthogonal code-set.

The reliability of a communication link is highly dependent on achieving a stable frame synchronization obtained through preamble detection. The preamble signal for the FSDT presented in [5] requires an $f_{3dB\text{-}BW}$ of 5.25 MHz for its chip rate, while the maximum information data rate is 1.3125 Mbps, thereby limiting the overall spectral efficiency to 0.25 bps/Hz. The preamble structures using the M-Sequence code [11] combined with the Walsh code presented in [9] and the Manchester-coded pseudorandom binary sequence (PRBS) used in [10] have good autocorrelation properties. However, they do not consider the spectral regulations in [12] regarding their wide bandwidths.

The proposed preamble structure consists of the four sub-preambles with the same first three sub-preambles for the coarse detection of the preamble location, and a different last preamble for the fine detection of the preamble start point, which can be fully utilized by the proposed detection algorithm to enhance the frame synchronization performance. The pre-processing for the compensation of the adverse band-limit effects by the transmit and receive filters, enables the preamble signal to use the same frequency band with that of the transmit data signal of the NBDT.

Section II describes the HBC system model. Section III deals with comparisons between the conventional FSDT and proposed NBDT. Section IV presents the proposed preamble structure along with its detection algorithm for the frame synchronization. The results of the performance evaluations are presented in Section V. The conclusion is given in Section VI.

II. HBC System Model

Figure 1 shows a signal transmission path model of HBC based on the FSDT when the data are transmitted from the wrist to the chest through the body. The transmitted signal in digital form passes through a transmit band-pass filter (TBPF)

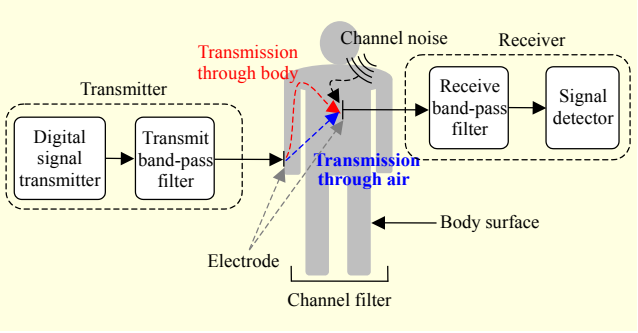

Fig. 1. Signal transmission path model.

to meet the TSM requirements before being induced into the human body through a signal electrode using, for example, a copper plate on a printed-circuit-board or an electrocardiogram monitoring electrode.

Human body channel modeling can be classified depending on its signal transmission method of capacitive coupling or galvanic coupling [13]. In capacitive coupling, only the signal electrode at both sides of the Tx and receiver (Rx) is attached to the human body, while the ground electrode remains floating. In the galvanic coupling method, both electrodes of the Tx and Rx sides are attached to the body. It has been shown that transmission using galvanic coupling achieves better performance than that of capacitive coupling only for a low frequency range of under 60 kHz at low data rates [14]. Hence, systems operating in the mega-hertz range of f_{op} are suitable for the capacitive coupling transmission. In capacitive coupling, the channel filter can be effectively composed of two paths, in the air and through the body, and modeled as a finite impulse response [15]–[17]. The channel path loss increases as the ground planes of the Tx and Rx become smaller, and the distances between the Tx and Rx become farther [15].

The channel noise sources are electromagnetic waves generated from various electronic devices around the user. These are absorbed into the human body due to the antenna effects of the human body [18], [19], where the power of the thermal noise at the Rx is negligible compared to that of the channel noise. The channel noise has a Gaussian distribution [15]. Hence, considering a linear discrete-time channel, the received signal can be represented as

$$y_k = \sum_{i=0}^{L-1} h_i m_{k-i} + n_k, \quad (1)$$

where y is an output, m is a binary input of {0, 1}, n is white Gaussian channel noise with a power spectral density (PSD) of σ^2, and h is a human body channel impulse response of a causal system with L multipath terms.

The Rx adopts a receive band-pass filter (RBPF) to improve the SNR in the signal detection process by removing noises outside the frequency band of the desired signals.

Table 1. Comparison of HBC data transmission schemes based on FSDT.

Work	Transmission scheme	f_{op} (MHz)	3 dB bandwidth (MHz)	Maximum data rate (Mbps)	Spectral efficiency (bps/Hz)	Compatibility with frequency allocation in [12]	Minimum HD of symbol code	η_{sg}
[5]	FSDT for IEEE standards	42	18.375–23.625	1.3125	0.2500	Yes	64	0.50
[7]	Parallelized multi-spreader	42	15.75–26.25	3.9375	0.3750	No	32	0.25
[8]	Parallelized multi-spreader	42	18.375–23.625	2.2969	0.4375	Yes	32	0.25
[9]	Multi-level baseband coding	160	N/A	60	N/A	No	4	0.25
[10]	Spreading with direct Walsh code mapping	32	8–22	2	0.1429	No	32	0.50
This work	Direct spreading using FSC	42	20.34375–21.65625	1.3125	1.0000	Yes	32	1.00

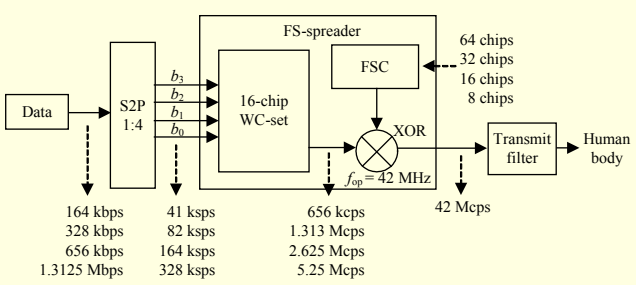

Fig. 2. Block diagram of FSDT transmitter.

III. Proposed Transmission Scheme

1. Previous HBC Transmission Schemes Based on FSDT

A block diagram of the FSDT Tx for a maximum data rate of 1.3125 Mbps using an f_{op} of 42 MHz is shown in Fig. 2 [5]. The baseband data pass through an S2P to form a 4-bit parallel signal. The 4-bit signal is mapped to the corresponding orthogonal code equivalent to the 16-chip Walsh code (WC), and then spread by applying a frequency shift code (FSC) of a [0 1] repeated code. For example, the 8-chip FSC code is [0 1 0 1 0 1 0 1]. The spread code, defined as a symbol-code, passes through a transmit filter to meet the TSM requirements.

Table 1 shows comparisons of previously published HBC data transmission schemes based on the FSDT for maximum data rates. Compared to the FSDT, the modified FSDT presented in [7] achieves three times the maximum data rate, but the transmit signal requires twice the expanded $f_{3dB\text{-}BW}$ of the TSM. The multi-level baseband coding scheme in [9] significantly improves the data rate up to 60 Mbps. However, it uses an approximately four-times higher f_{op} of 160 MHz, and the minimum HD of the symbol-code is reduced to 4. Neither scheme contributes to BER performance enhancement, nor do they consider the regulations of the frequency allocations [12]. In [8], the data rate can be increased to 75%, at the expense of a 50% reduction in the minimum HD of the symbol-code. The maximum data rate of the NBDT is desirable for use in the on-body applications listed in [3] having a data rate typically in the range of kbps.

2. Proposed HBC Transmission Scheme of NBDT

Figure 3 shows a block diagram of the NBDT Tx. Compared to the FSDT Tx shown in Fig. 2, the NBDT Tx is simplified by excluding the S2P and the memory for storing the 16-chip WC-set. The data bit b_0 is directly spread by the FSC without a bit-to-WC mapping process. Hence, the bit transient of b_0 only incurs the RBPs resulting in a reduction of the number of RBPs in the transmitted signal. The symbol-code lengths of the FSDT and NBDT are 16 × the length of the FSC, and the length of the FSC itself, respectively. While the symbol-code length of the NBDT is reduced to one-quarter that of the FSDT for the same data rate, the symbol-code of the NBDT can secure one-half of the minimum HD compared to that of the FSDT due to the orthogonality of the code. If a spreading-gain efficiency η_{sg} for the FSDT based transmission schemes is defined as

$$\eta_{sg} = \frac{\text{Minimum HD of symbol-code}}{\text{Length of symbol-code}}, \quad (2)$$

then it can be seen in Table 1 that the NBDT achieves the highest efficiency in obtaining HD for detecting a symbol-code,

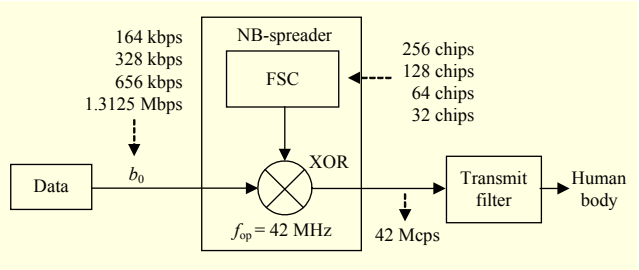

Fig. 3. Block diagram of NBDT transmitter.

ETRI Journal, Volume 38, Number 6, December 2016
http://dx.doi.org/10.4218/etrij.16.2716.0003

where the length indicates the number of chips.

3. Transmit Signal Analysis

As shown in Fig. 4, the FSDT and NBDT transmitted signals are mostly distributed around 21 MHz in the frequency domain, where T is the sampling rate and V is the binary 1 voltage level. Although filters can be implemented through various design rules, and the performances of the filtered signals are determined based on the individual optimization processes, this work is mainly concentrated on performance comparisons between the conventional and proposed schemes on the effects of compliance with the TSM. Hence, the TBPF was designed to exactly fit the FSDT transmitted signals into the TSM without redundant margins so as to minimize signal distortions in the transmitted signals. The RBPF is employed to improve the SNR by rejecting noise while minimizing distortions in the desired signals. Figure 5 shows the frequency responses of the TBPF and RBPF with the parameter values, where f_s is the sampling frequency, and f_{c1} and f_{c2} are the lower and upper cut-off frequencies, respectively. These filters were designed as a Butterworth infinite impulse response (IIR) filter type for its flatness of frequency response in the pass-band, and to be compatible with the designs using analog filters.

While the maximum data rate of the FSDT is 1.3125 Mbps, the $f_{3dB\text{-}BW}$ of the TSM is 5.25 MHz, as shown in Fig. 4(a), where the TSM achieves –120 dBr, –80 dBr, –25 dBr, –34 dBr, and –75 dBr at 1 MHz, 2 MHz, 50 MHz, 105 MHz, and 400 MHz, respectively [5]. The maximum spectral efficiency of the FSDT is limited to 0.25 bps/Hz. The NBDT can reduce its $f_{3dB\text{-}BW}$ to 1.3125 MHz by satisfying the reduced-bandwidth TSM, where the $f_{3dB\text{-}BW}$ of the TSM is narrowed from 5.25 MHz to 1.3125 MHz, as shown in Fig. 4(b). Hence, the NBDT achieves a spectral efficiency of up to 1 bps/Hz based on the $f_{3dB\text{-}BW}$ of the TSM, which is four-times greater than that of the FSDT, and improves the availability to share the spare frequency band with the independent transmissions for more than two transceiver pairs of on-body applications for WBANs [3].

Figure 6 shows the ISI effects on the FSDT signals after passing through the TBPF and both the TBPF and RBPF, where the average channel loss is assumed to be approximately –40 dB, and the filter delays of the received signals are compensated. Because filtering the observed signal results in the transmitted signal becoming band-limited, the RBPs of a series of 0 s and 1 s in the transmitted signals induce the ISI after the transmit filtering [7], and every second chip of the RBPs will be falsely detected in the Rx. The average number of RBPs in one symbol-code derived from the 16-chip WC-set of the FSDT is 7.5. Hence, the BER performance is expected

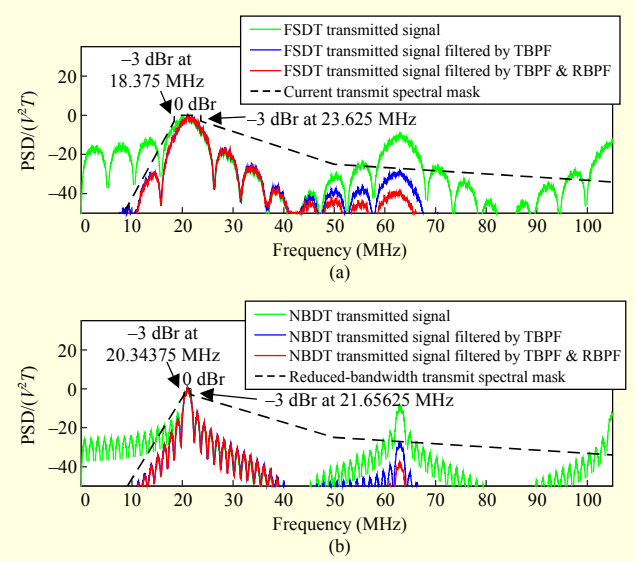

Fig. 4. Transmit power spectrums of transmitted signal, transmitted signal filtered by TBPF, and transmitted signal filtered by TBPF and RBPF for maximum data rate of 1.3125 Mbps with TSM: (a) Transmit power spectrums of FSDT with the current TSM. (b) Transmit power spectrums of NBDT with the reduced-bandwidth TSM.

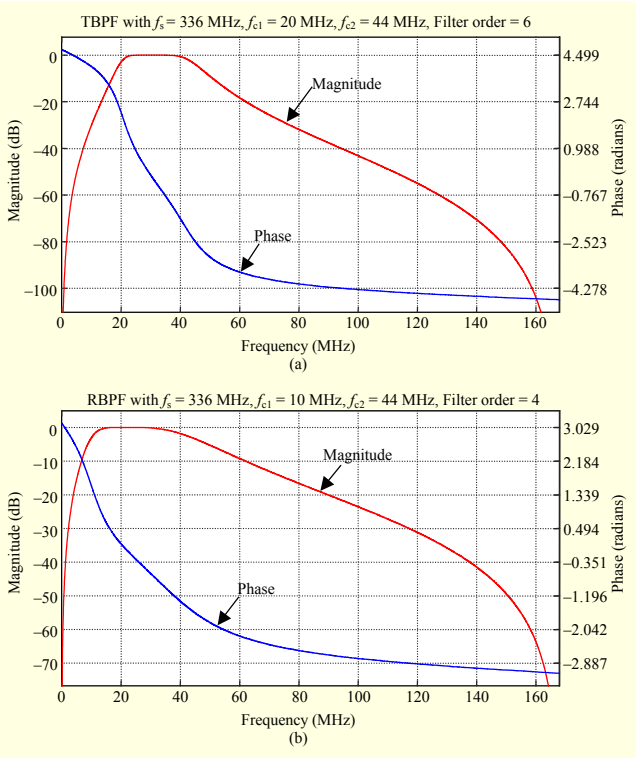

Fig. 5. Frequency responses of filters: (a) TBPF. (b) RBPF.

to be degraded by the effects of the transmit filter. In the case of the NBDT, the RBP is not included in the symbol-code, but only occurs when the binary value of consecutive b_0 is inverted

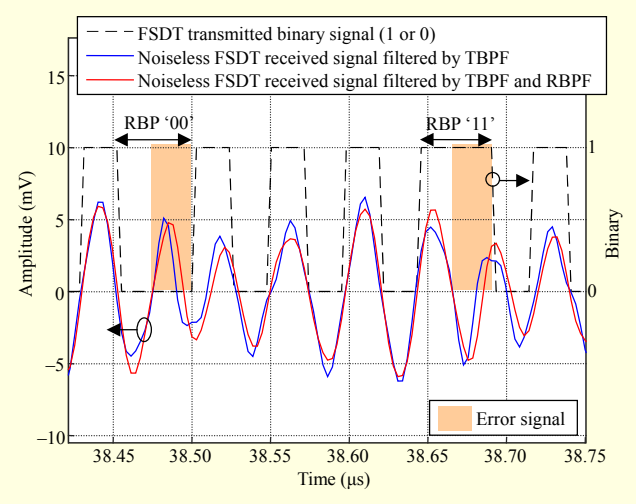

Fig. 6. Noiseless FSDT received signals passed through filters.

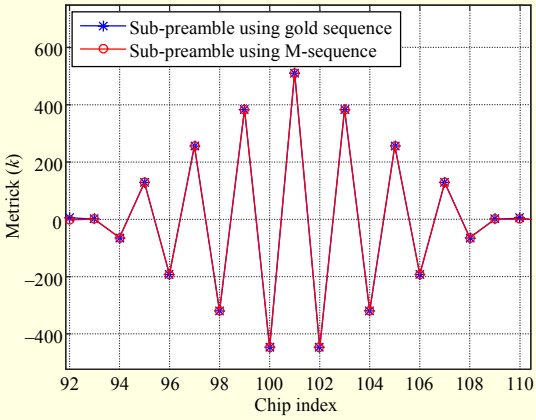

Fig. 7. Autocorrelations for sub-preambles created by gold sequence and M-sequence with time-delay of 100 chips.

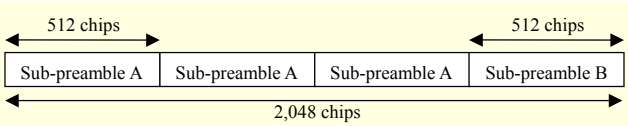

Fig. 8. Block diagram for proposed preamble generation.

from 0 to 1 or from 1 to 0.

IV. Proposed Preamble Structure with Detection Algorithm

The frequency properties of the preamble signal for frame synchronization should be identical to those of the transmit data signal, such as the center frequency, bandwidth, and shape of the PSD, to fit with the TBPF and RBPF. The center frequency of the preamble signal can be shifted by spreading a PRBS using an FSC with a given f_{op} of 42 MHz, and the bandwidth can be adjusted by the ratio of the lengths between the PRBS and FSC. In the NBDT, the NB-spreader in Fig. 3 can be shared to transmit the preamble as the data changes to a PRBS.

The preamble structure for the FSDT presented in [5] is formed by four times the number of repetitions of the same 512-chip sub-preamble created by spreading a 64-bit gold sequence using the 8-chip FSC. With the given length of the preamble, the repetitions of a short sub-preamble can reduce the bandwidth, and improve the detection performance through the repetition diversity gain. In the Rx, the optimum maximum likelihood (ML) detector, calculating the preamble autocorrelation values for every chip index to find the chip index having the maximum correlation value, is infeasible due to its considerable complexity, where the autocorrelation is calculated as

$$\text{Metric}(k) \equiv \sum_{i=0}^{D-1} P_i z_{k+i}, \quad (3)$$

where Metric(k) is the correlation value at the kth chip index of the time-delay, z is the hard-decision received signal of y in (1), P is a preamble with a length of D, and the binary value of 0 in P and z is mapped to –1. The alternative detection method presented in [20] compares the predefined threshold to Metric(k) using the sub-preamble as P, and selects the chip index where Metric(k) is higher than the threshold value. It finds the four start chip indexes of the corresponding individual sub-preambles with consideration of the intervals between each start chip index, where the interval between each start chip index is 512. Figure 7 shows the autocorrelations of 512-chip sub-preambles using the 64-bit gold sequence in [5] and a 64-bit PRBS, where the 64-bit PRBS is generated from a 63-bit M-sequence using the generator polynomial of $p(z) = z^6 + z^5 + 1$ followed by an additional 0, the length of FSC is 8, and the time-delay is 100 chips. Whereas the gold sequence is constructed through the XOR operation of two M-sequences requiring more complexity than that of the M-sequence generation, the differences in the autocorrelation properties between the sub-preambles using the gold sequence and M-sequence are not observable. The maximum peak value is the same as the length of the sub-preamble, and the differences in the autocorrelation values between two neighboring peaks are the same as twice the length of the applied random sequence due to the use of bipolar signals. The additional FSC–2 numbers of peaks are caused by the spreading process. The neighboring peaks around the desired chip index worsen the performance in the threshold detection and narrow the range of the proper threshold values. Hence, to overcome the performance loss by the neighboring peaks, this paper proposes a threshold detection method combined with the ML detection within a limited range of the chip index, defined as mixed-detection, with adaptive modifications of the preamble structure.

Figure 8 shows a block diagram of the proposed preamble

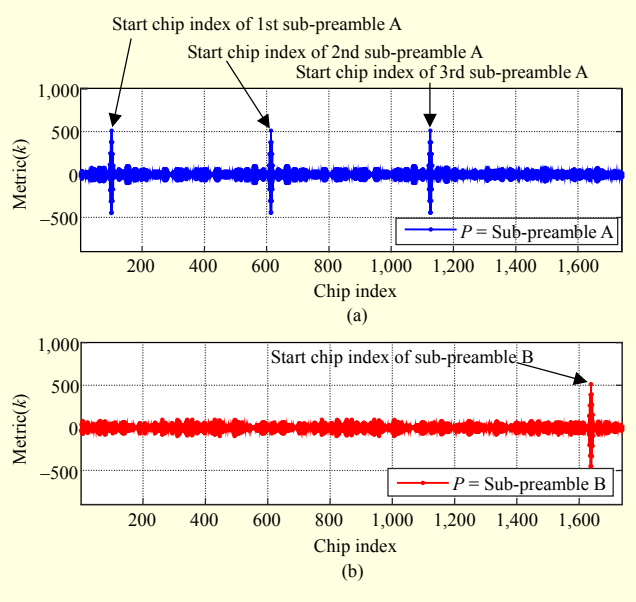

Fig. 9. Metric(k) for y of proposed preamble signal with time-delay of 100 chips: (a) Applying sub-preamble A as P. (b) Applying sub-preamble B as P.

generation. The first three sub-preamble As, are created using the same PRBS, but the last sub-preamble B uses a different PRBS from that of the sub-preamble A. For example, the sub-preamble A and sub-preamble B can be generated from the 1st through the 64th and the 65th through the 128th bits of a 128-bit PRBS, respectively, where the 128-bit PRBS is composed of a 127-bit M-sequence using the generator polynomial of $p(z) = z^7 + z^6 + 1$ and an additional 0. The chip length of each sub-preamble is 512 by spreading the PRBSs through the 8-chip FSC. Figures 9(a) and 9(b) show Metric(k)s when y is the proposed preamble signal with a time-delay of 100 chips, and Metric(k)s of Figs. 9(a) and 9(b) apply sub-preamble A and sub-preamble B, respectively, as P. With these autocorrelation properties, the mixed-detection is composed of the threshold detections applied to find the sub-preamble As for the coarse detection of the preamble location, and the subsequent ML detection to find the sub-preamble B for the fine detection of the preamble start chip index. The main rule of the preceding coarse detection process is to limit the computation range of the ML detection.

Figure 10 presents a flowchart describing the proposed algorithm for the mixed-detection, where Q is a predefined autocorrelation threshold, and the variables i, j, x, and w indicate the chip indexes. In Step 1, when Metric(k) using sub-preamble A as P is larger than Q, the detection process assumes that the first or second sub-preamble A is found. It stops computing and moves to Step 2-1. In Step 2-1, Metric(k) is calculated within the range of x from $i + D$ up to $i + D + 2j$ because Metric(i) in Step 1 might detect one of the previous peaks in Fig. 7, which is not exactly the desired peak, where j can be fixed at 3 due to the three neighboring peaks from the 8-chip FSC. If Metric(x) is larger than Q, the detection process supposes that the detector finds the first and second sub-

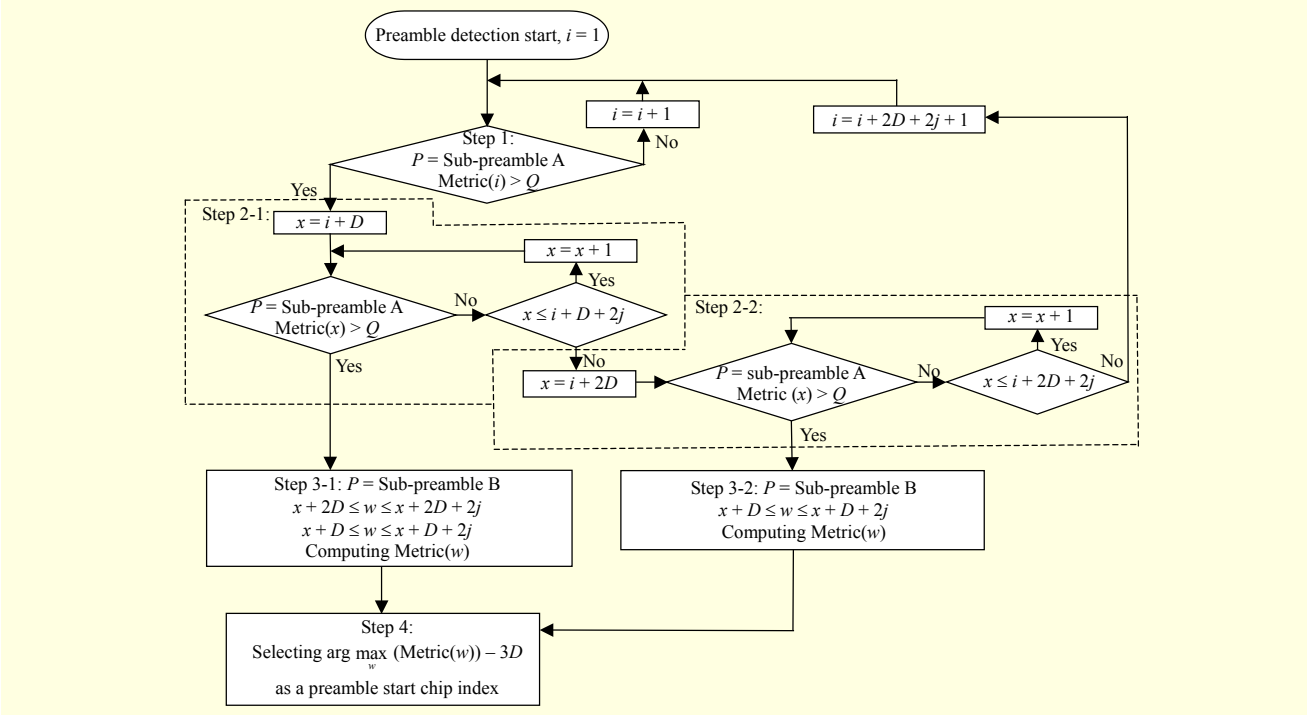

Fig. 10. Flowchart illustrating proposed algorithm for preamble detection.

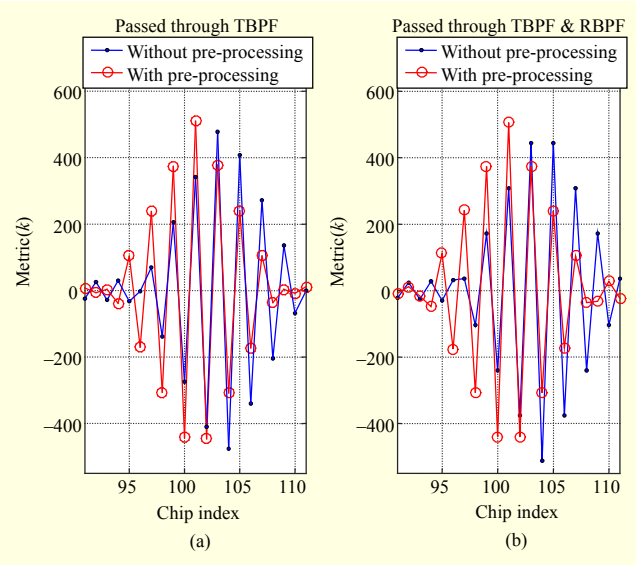

Fig. 11. Metric(k) for P of sub-preamble A, and y of sub-preamble A passed through corresponding filters, for without and with proposed pre-processing, for given time-delay of 100 chips: (a) For y passed through TBPF. (b) For y passed through TBPF and RBPF.

preamble A, or the second and third sub-preamble A. It stops computing Metric(x), and moves to Step 3-1 for the ML detection. The detection process computes Metric(w) using sub-preamble B as P within the two given ranges, where the upper range is for the case in which the first and second sub-preamble As are found in the previous Steps, and the lower range is for the case in which the second and third sub-preamble As are found. In Step 4, the preamble start chip index is obtained by subtracting $-3D$ from w having the maximum value of Metric(w). If the conditions in Step 2-1 are not satisfied, Metric(x) is computed within the range of $i + 2D$ to $i + 2D + 2j$ in Step 2-2 to find the third sub-preamble A. If an x satisfying the conditions in Step 2-2 exists, the detector assumes that the first and third sub-preamble As are found. The ML detection is applied within the range of $x + D$ to $x + D + 2j$ to find the start chip index of the sub-preamble B in Step 3-2, which is followed by Step 4.

The properties of the PSD of the proposed preamble signal are identical to those of the transmit data signal of the FSDT with a maximum data rate of 1.3125 Mbps because the chip rate of the preamble before spreading by the 8-chip FSC with an f_{op} of 42 MHz is 5.25 Mcps. Hence, the preamble transmit signal requires an $f_{3dB\text{-}BW}$ of 5.25 MHz regardless of the $f_{3dB\text{-}BW}$ of the information data rate. The TBPF and RBPF currently designed for the transmit data signal of the NBDT are expected to cause the band-limit effects on the preamble signal and induce the chip errors on the RBPs in the preamble. Figure 11 shows Metric(k)s when P is the sub-preamble A, and ys are the sub-preamble As passed through the TBPF and both the TBPF and RBPF, respectively, for without and with the proposed pre-processing. When there is no pre-processing, as shown in the blue curves in Figs. 11(a) and 11(b), the maximum peak of Metric(k) cannot point to the correct chip index of the sub-preamble start, with a given time-delay of 100 chips, due to the errors in the RBPs.

If the filters are implemented once, the filter responses are fixed, and the positions where the chip errors occur are also predetermined. The proposed pre-processing adopts the hard-decision binary signal obtained from the sub-preamble passed through the corresponding filters as P instead of the original transmitted sub-preamble, in the detection process. As shown in the red curves in Figs. 11(a) and 11(b), Metric(k) with the pre-processing applied can detect the correct chip index of the sub-preamble start with the maximum value of Metric(k).

V. Performance Evaluation

The channel model document for WBANs [15] deals with the impulse response h in (1) for the HBC in terms of the sizes of the ground planes of the Tx and Rx and the distances between the Tx and Rx. It has been shown that the root mean square delay spread of h is sufficiently smaller than that of the chip rate for the FSDT with an f_{op} of 42 MHz [7], [15]. The ISI effects by the channel filter on the transmitted signal are negligible compared to those by the TBPF. Hence, h is approximated as a one-tap filter of unity gain in this paper.

1. BER Performance

In the Rx, the received signal can be determined to be a binary signal by using a comparator and a clock-and-data recovery in the analog front end (AFE) [9], [10], [21]. With the assumption of perfect frame synchronization, an ML detector calculates the HD between the hard-decision bit stream from the AFE, and all of the candidate symbol-code vectors, and finds the candidate code vector $\hat{\mathbf{c}}$ satisfying

$$\hat{\mathbf{c}} = \arg\min_{\mathbf{c}\in S} \mathrm{d}(\mathbf{c}, \mathbf{z}), \tag{4}$$

where S denotes the set of candidates of symbol-code vectors, d( ) is the HD between two vectors, and $\mathbf{z}$ is the code vector of the hard-decision received signal. The HD computation can be carried out using XOR operation and counting the number of 1s of the two code vectors. Table 2 shows a comparison of the detection complexity of the length of the HD computations for one information bit between the FSDT and NBDT. The NBDT can reduce the length of the HD computations to 12.5 % that of the FSDT. When the data rate is 164 kbps, the number of bitwise XORs and bitwise counts is maximally reduced by

Table 2. Comparison of detection complexity.

Data rate (Mbps)	Symbol-code length		Length of HD computation per information bit	
	FSDT (l_{FSDT})	NBDT (l_{NBDT})	FSDT ($\frac{l_{FSDT} \times n_{FSDT}}{4}$ [1])	NBDT ($l_{NBDT} \times n_{NBDT}$ [2])
0.164	1,024	256	4,096	512
0.328	512	128	2,048	256
0.656	256	64	1,024	128
1.3125	128	32	512	64

1) Number of candidate symbol-codes of FSDT = 16.
2) Number of candidate symbol-codes of NBDT = 2.

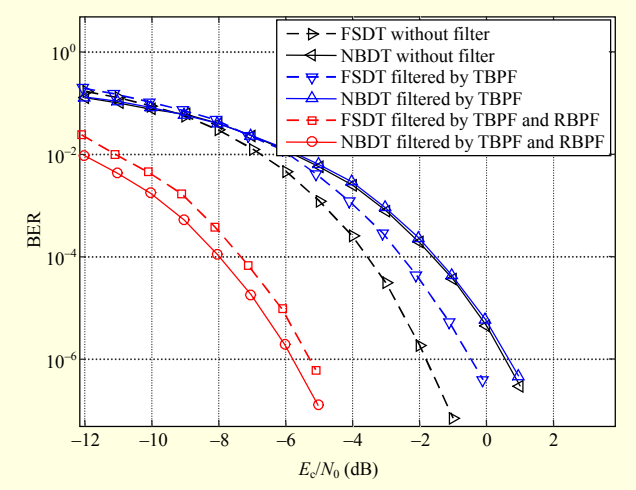

Fig. 12. BER performance curves of FSDT and NBDT for maximum data rate of 1.3125 Mbps in AWGN channel.

3,584 from 4,096 to 512.

Figure 12 shows the BER versus the received energy per chip over the channel noise PSD (E_c/N_0) curves for the FSDT and NBDT for a maximum data rate of 1.3125 Mbps with respect to the effects of the TBPF and RBPF in the AWGN channel. If the data rate is halved, the BER performance is expected to improve by increasing in the minimum number of error chips occurring the symbol error [18]. Without filtering, the values of E_c/N_0 required to achieve a BER of 10^{-6} are about –1.81 dB and 0.56 dB for the FSDT and NBDT, respectively. The NBDT degrades the required E_c/N_0 by approximately 2.37 dB compared to the FSDT when the filters are not applied. The BER performance of the FSDT is degraded by about 1.35 dB at a BER of 10^{-6} when the TBPF is applied. However, the performance degradation of the NBDT with the TBPF is less than 0.1 dB. This result shows the robustness of the NBDT against the effects of the transmit filter. The FSDT and NBDT with both the TBPF and RBPF improve the SNR by about 4.82 dB and 6.45 dB respectively, at a BER of 10^{-6}. While the main frequency bands of the FSDT and NBDT transmitted signals appear to be little affected by the RBPF, as shown in Figs. 4(a) and 4(b), the effective SNR gain of the NBDT obtained by the RBPF results in a 1.63 dB higher than that of the FSDT since the error chips by the ISI on the RBPs of the FSDT symbol-code cannot be recovered by simply increasing the signal power. As shown by the two red curves, the NBDT can improve the SNR by about 0.51 dB at a BER of 10^{-6}, compared to the FSDT.

To verify the availability of spectrum sharing with independent channels within the given bandwidth for the NBDT related to Fig. 4(b), performance simulations in terms of the multiple transmissions were conducted, and the performance results were compared to those of the FSDT related to Fig. 4(a). According to the properties of the FSDT and NBDT, the center frequency is determined by half of f_{op}, and the data rate increases linearly with an increase in the f_{op} if the length of the symbol-code is fixed. Considering the resolution limit of frequency division by discretization, the center frequencies are determined as integer values, and the simulations are conducted in two channels of the center frequencies of 20 MHz and 22 MHz satisfying the TSM for the HBC in the standards. The channel1 (ch.1) and channel2 (ch.2) of the NBDT and FSDT are allocated to the center frequencies of 20 MHz with the data rate of 1.25 Mbps and 22 MHz with the data rate of 1.375 Mbps, respectively, as shown by the transmit power spectrums in Fig. 13. The TBPF for the multi-transmission (TBPF-multi) is designed that f_s is 440 MHz, and f_{c1} and f_{c2} are 16 MHz and 40 MHz, respectively, using the type

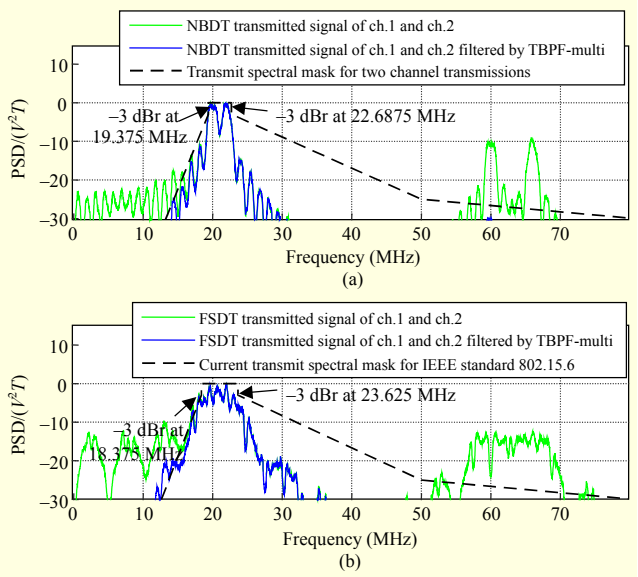

Fig. 13. Transmit power spectrums of multiple transmissions of NBDT and FSDT: (a) Transmit power spectrums of NBDT with TSM for two channel transmissions. (b) Transmit power spectrums of FSDT with current TSM.

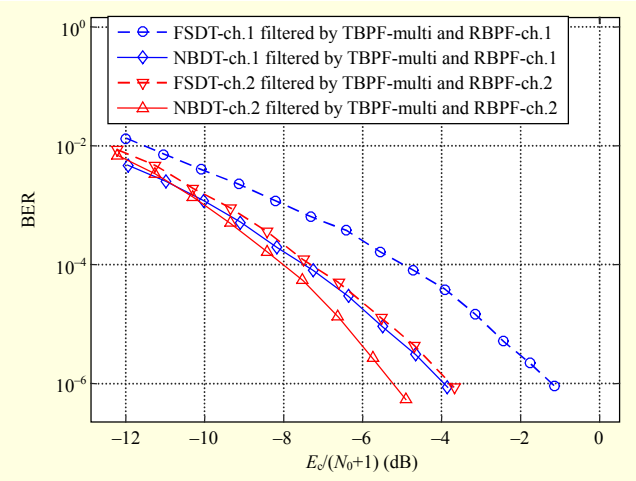

Fig. 14. BER performance curves of FSDT and NBDT for two channel transmissions for normalized data rate of 1.3125 Mbps in AWGN channel.

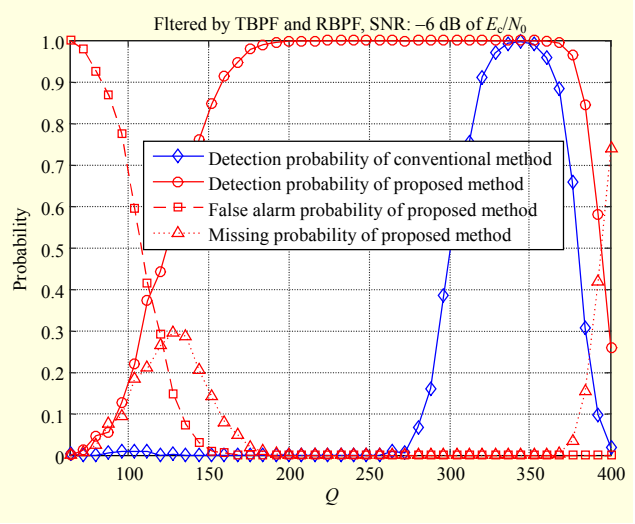

Fig. 15. Performances of frame synchronization for conventional FSDT preamble using threshold detection and proposed preamble using mixed-detection in AWGN channel.

of a 6th order IIR Butterworth filter. The $f_{3dB\text{-}BW}$ of the NBDT transmit signal filtered by the TBPF-multi is approximately 3.3125 MHz from 19.375 MHz to 22.6875 MHz. Hence, the spectral efficiency is measured as 2.625 Mbps/3.3125 MHz = 0.7925 bps/Hz including the guard band between the two channels spaced by the integer-valued center frequencies. The same TBPF-multi is applied to the FSDT for the performance comparisons under the same filtering condition, while the TBPF-multi for the FSDT should be narrowed, leading to performance degradation, to satisfy the transmitted signal with the current TSM as shown in Fig. 13(b), where the signals in a frequency range of approximately 11 MHz to 14 MHz exceed the current TSM.

Figure 14 shows the BER versus the received energy per chip of desired signal over the power of the channel noise plus the channel interference ($E_c/(N_0 + I)$) results for the multiple transmissions for the FSDT and NBDT, where the transmission channels are allocated as shown in Fig. 13, the signals of the two channels have the same transmit power, the phase differences of the two channel signals are determined at random, and the BER performances are calibrated to the normalized data rate of 1.3125 Mbps. The f_{c1} and f_{c2} of the RBPF, using the type of a 4th order IIR Butterworth filter for ch.1 (RBPF-ch.1), are 10 MHz and 21 MHz, respectively, and those of the RBPF-ch.2 are 21 MHz and 40 MHz, respectively. The performance degradation of ch.1 is greater than that of ch.2 for both the FSDT and NBDT, because the signal rejections on ch.1 are more severe than those of ch.2 due to the narrower pass band of the RBPF-ch.1 than that of the RBPF-ch.2. Compared to the FSDT, the NBDT can lessen the performance loss, caused by channel interference and signal rejections by the filters, by about 2.73 dB and 1.46 dB for the ch.1 and ch.2, respectively. It shows that the NBDT, with higher spectral efficiency, improves tolerance to the effects from multiple transmissions.

2. Frame Synchronization Performance

Figure 15 shows the performance results of frame synchronization for the conventional FSDT preamble [5] using the threshold detection [20], and the proposed preamble using the mixed-detection, with applying the pre-processing, in the AWGN channel, where the detection probability is defined as the probability that the detector correctly detects the start chip index of the preamble with a given time-delay, the false alarm probability is defined as the probability that the detector detects an incorrect start point of the preamble including even the case when the preamble signal is actually absent, and the missing probability is defined as the probability that the detector misses a preamble when the preamble signal is actually present. The transmitted frame for the simulation consists of the preamble, 256 random NBDT symbol-codes, and nulls for the same time period of the symbol-codes. The transmit and receive signals are filtered using the TBPF and RBPF, respectively. Perfect frame synchronization should be guaranteed at the E_c/N_0 of about –6 dB for achieving a BER of 10^{-6} of the information data as shown in Fig. 12. In addition, a Q value with a wide range is required for perfect frame synchronization, because the proper threshold value is easy to vary with the channel noise power. The results were obtained from 10,000 trials of frame detections per each Q value increasing at a step size of 8. The detection probability curves show that the proposed method can achieve a preamble detection probability of 1 for the wider range of Q from 232 to 344, compared to that of the

conventional method.

VI. Conclusion

This paper presented a bandwidth-efficient, and both BER and synchronization performance-enhanced transmission scheme for the HBC, with a highly simplified structure and compatibility with the spectral regulation for WBANs. The proposed NBDT improves the spectral efficiency by a factor of 4 and the required SNR by about 0.51 dB at a BER of 10^{-6} with a significant reduction of the length of the HD computation in the ML detection process to 12.5%, compared to those of the conventional FSDT. It was verified that the proposed preamble structure and the mixed-detection algorithm by applying the pre-processing scheme secure the perfect frame synchronization at the SNR of about –6 dB, which is the SNR required to achieve a BER of 10^{-6} for the information data, for a wide range of Q.

References

[1] T.G. Zimmerman, "Personal Area Networks: Near-field Intrabody Communication," *IBM Syst. J.*, vol. 35, no. 3.4, 1996, pp. 609–617.

[2] T.G. Zimmerman et al., "Applying Electric Field Sensing to Human-Computer-Interfaces," *Proc. SIGCI Conf. Human Factors Comput. Syst.*, Denver, CO, USA, 1995, pp. 280–287.

[3] S. Movassaghi et al., "Wireless Body Area Networks: a Survey," *IEEE Commun. Surveys Tuts.*, vol. 16, no. 3, 2014, pp. 1658–1686.

[4] C.H. Hyoung et al., "A Novel System for Intrabody Communications: Touch-and-Play," *IEEE Int. Symp. Circuit Syst.*, Kos, Greece, May 21–24, 2006, pp. 1343–1346.

[5] *IEEE Standard for Llocal and Metropolitan Area Networks—Part 15.6: Wireless Body Area Networks*, IEEE 802.15 working group for WPAN, 2012.

[6] C.H. Hyoung et al., "A Feasibility Study on the Adoption of Human Body Communication for Medical Service," *IEEE Trans. Circuits Syst. II: Exp. Briefs*, vol. 62, no. 2, 2015, pp. 169–173.

[7] T.W. Kang et al., "A Method of Increasing Data Rate for Human Body Communication System for Body Area Network Applications," *IEEE Veh. Technol. Conf.*, Quebec, Canada, Sept. 3–6, 2012, pp. 1–5.

[8] T.W. Kang et al., "Improving Data Rate in the Human Body Communications," *Int. Conf. Inform. Commun. Technol. Convergence*, Busan, Rep. of Korea, Oct. 2014, pp. 51–52.

[9] C.K. Ho et al., "High Bandwidth Efficiency and Low Power Consumption Walsh Code Implementation Methods for Body Channel Communication," *IEEE Trans. Microw. Theory Techn.*, vol. 62, no. 9, Sept. 2014, pp. 1867–1878.

[10] C.H. Hyoung et al., "Transceiver for Human Body Communication Using Frequency Selective Digital Transmission," *ETRI J.*, vol. 34, no. 2, Apr. 2012, pp. 216–225.

[11] J.G. Proakis, *Digital Communications*, New York, USA: McGraw Hill, 2001.

[12] IEEE 802.15-10-0318-00-0006, *Supplemental Information for HBC*, May 2010.

[13] M.H. Seyedi et al., "A Survey on Intrabody Communications for Body Area Network Applications," *IEEE Trans. Biomed. Eng.*, vol. 60, no. 8, Aug. 2013, pp. 2067–2079.

[14] M.A. Callejon et al., "A Comprehensive Study Into Intrabody Communication Measurements," *IEEE Trans. Instrum. Meas.*, vol. 62, no. 9, Sept. 2013, pp. 2446–2455.

[15] IEEE P802.15-08-0780-12-0006, *Channel Model for Body Area Network (BAN)*, Nov. 2010.

[16] J.H. Hwang et al., "Empirical Channel Model for Human Body Communication," *IEEE Antennas Wireless Propag. Lett.*, vol. 14, 2015, pp. 694–697.

[17] J.H. Hwang et al., "Measurement of Transmission Properties of HBC Channel and Its Impulse Response Model," *IEEE Trans. Instrum. Meas*, vol. 65, no. 1, Jan. 2016, pp. 177–188.

[18] J.H. Hwang et al., "Analysis on Co-channel Interference of Human Body Communication Supporting IEEE 802.15.6 BAN Standard," *ETRI J.*, vol. 37, no. 3, June 2015, pp. 439–449.

[19] J.H. Hwang et al., "Energy Harvesting from Ambient Electromagnetic Wave Using Human Body as Antenna," *Electron. Lett.*, vol. 49, no. 2, Jan. 2013, pp. 149–151.

[20] H.K. Choi et al., *Communication Apparatus and Method Using Pseudo-Random Code*, US Patent 13/696,740, filed May. 7, 2010.

[21] V.V. Kulkarni et al., "A Reference-Less Injection-Locked Clock-Recovery Scheme for Multilevel-Signaling-based Wideband BCC Receivers," *IEEE Trans. Microw. Theory Techn.*, vol. 62, no. 9, Sept. 2014, pp.1856–1866.

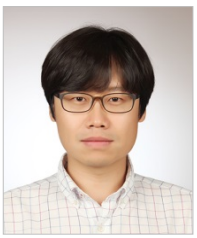

Tae-Wook Kang received the BS and MS degree, in electrical engineering from Pohang University of Science and Technology Rep. of Korea, in 2005 and 2007, respectively. Since February 2007, he has been with ETRI, Daejeon, Rep. of Korea, where he is currently a Senior Engineer. He has been primarily involved in human body communications. His research interests include wireless communications, channel modeling and power management of energy harvesting systems.

Jung-Hwan Hwang received the BS and MS degrees in electronic engineering from Chungnam National University, Daejeon, Rep. of Korea, in 1998 and 2000, respectively, and the PhD degree in information and communication engineering from the Korea Advanced Institute of Science and Technology, Daejeon, Korea, in 2016. From March 2000 to July 2002, he was a Research Engineer with Knowledge-on Inc., Iksan, Rep. of Korea, working on the development of microwave circuits. Since August 2002, he has been with the ETRI, Daejeon, Rep. of Korea, where he is currently a Senior Engineer. He has been primarily involved in the radio channel modeling. His research interests include EMC (Electromagnetic Compatibility), electromagnetic fields safety and health effects.

Sung-Eun Kim received the BS degree in electrical & computer engineering from Hanyang University, Seoul, Rep. of Korea, in 2002, and the MS degree in electrical engineering from the KAIST, in 2004. Since March 2004, he has been with the ETRI, where he is currently a Senior Engineer. He has been primarily involved in researching analog circuit design for human body communications, and power management of energy harvesting systems.

Kwang-Il Oh received the BS degree in electrical engineering from Kyungpook National University, Daegu, Rep. of Korea, in 2002, and the MS and PhD degrees in electrical engineering from the KAIST, in 2004 and 2009, respectively. From March 2009 to February 2015, he was a senior engineer at Silicon Works Co., Ltd., Daejeon, Rep. of Korea, where he was involved in the high-bandwidth interface circuits design for LCD modules. Since March 2015, he has been with the ETRI, where he is involved in analog circuit design. His interests include high performance amplifiers, CDRs, DLL/PLL circuits, and signal integrity.

Hyung-Il Park received the BS and MS degrees in electronic engineering from Chonnam National University, Gwangju, Rep. of Korea, in 1995 and 1997, respectively. From March 1997 to August 1999, he was a Research Engineer with Anam Semiconductor Technology Inc., Seoul, Rep. of Korea, working on the development of RISC processors. Since September 1999, he has been with the ETRI, where he is currently a Research Director. He has been primarily involved in the development of baseband modems. His research interests include wireless communications, human body communications, and wearable computing systems.

In-Gi Lim received the BS and MS degrees in electronics engineering from Hanyang University, Seoul, Rep. of Korea, in 1987 and 1989, respectively, and the PhD degree in electronics engineering from Chungnam National University, Daejeon, Rep. of Korea, in 2005. Since 1989, he has been with the ETRI, where he is currently a Principal Researcher. He has been primarily involved in researching the wireless communications and human body communications.

Sung-Weon Kang received his BS and MS degrees in electronic engineering from Kyungpook National University, Daegu, Rep. of Korea, in 1987 and 1989, respectively, and his PhD in electrical engineering from the KAIST, in 2004. Since 2002, he has been with ETRI, where he is currently a principal engineer and the executive director of the Intelligent Semiconductor Research Department. His research interests include body area network (BAN) communication technology, RF MMICs, MEMS devices, nano-scale device modeling, artificial-intelligence SoC, machine learning and simulations. He was a reviewer for the IEEE Electron Devices Society. He has been a member of the Semiconductor Equipment and Materials Institute (SEMI) since 1993.